

Negative differential conductance and chiral effects in graphene field-effect transistors

A. Alarcon^{*}, V. Hung Nguyen^{*†}, J. Saint-Martin^{*}, A. Bournel^{*} and P. Dollfus^{*}

^{*}Institute of Fundamental Electronics, CNRS, Univ. Paris Sud, UMR8622, Orsay, France

[†]Center for Computational Physics, Institute of Physics, VAST, Hanoi, Vietnam

e-mail: alfonso.alarcon@u-psud.fr

Recently, it has been shown that graphene reported on hexagonal boron nitride (*h*-BN) provides higher mobility than on any other substrate [1,2], which makes possible to reach the ballistic transport regime even at room temperature. Additionally, in the case of Bernal stacking on *h*-BN, a small bandgap may open in graphene [3,4]. In this work we present a numerical study of the electrical behavior of top-gated monolayer graphene field-effect transistors (GFETs) wherein *h*-BN is used as substrate and gate insulator material (Fig. 1(a)). In addition to the strong influence of the chiral nature of carriers, it is shown that a negative differential conductance (NDC) may be achieved. Our model is based on the Green's function approach to solving the nearest-neighbour tight-binding Hamiltonian of graphene [5] self-consistently coupled with the 2D Poisson equation.

In Fig. 1(b) we plot a typical potential profile U_g and the local density of states (LDOS) for a particular value of the transverse momentum k_y , and an energy gap $E_{GAP}=0$. The corresponding transmission coefficient is displayed in Fig. 1(c). These figures illustrate well two important effects: (i) the transmission gap around the top of the barrier, which originates from the gap in the energy dispersion appearing at given k_y [6], and (ii) the chiral tunnelling through the barrier via the hole states. In the case of short gate length, the quantization of these hole states are likely to give rise to Klein tunnelling and resonant effects [7].

The drain current of a 50 nm gate length device is plotted in Fig. 2 as a function of the drain bias V_{DS} for different values of E_{GAP} in graphene [3,4], and for the temperatures $T=77$ K and $T=300$ K. An NDC effect is observed and it is strongly dependent on the value of the BN-induced bandgap in graphene and by the value of

temperature. The NDC arises when the transmission gap at the top of the barrier enters the window $[E_{FS}-E_{FD}]$ [8]. The peak-to-valley ratio can reach ≈ 3 for $E_{GAP}=100$ meV at $T=77$ K.

In Fig. 3(a) we show different curves of the current density as a function of the gate voltage, V_{GS} , for different gate lengths L_G . The minimum value of current, called Dirac point, corresponds to the transition between normal transmission above the barrier and chiral tunnelling through the barrier. It is controlled by the transmission gap which is L_G -dependent. It is also obviously dependent on E_{GAP} , as shown in Fig. 3(b). The I_{on}/I_{off} current ratio reaches ≈ 30 at $T=77$ K for $E_{GAP}=100$ meV and $L_G=50$ nm. At short gate length, oscillations of current are observed in the negative V_{GS} branch (Fig. 3(a)). They result from the quantization of hole states in the gated region which gives rise to resonant chiral tunnelling [9].

A zoom of Fig. 3(a) around of the Dirac point is shown in Fig. 4 for two values of the gate insulator thickness: $W_t=2$ nm and $W_t=10$ nm. When reducing L_G , a shift of the Dirac points to negatives V_{GS} values is observed. It is stronger when increasing W_t . This short channel effect is in full agreement with experimental results [10].

In summary, this study provides an understanding of the different transport behaviors of graphene field-effect transistors on *h*-BN substrate which is expected to make possible the recovering of the excellent intrinsic transport properties of graphene, with high potential of ballistic transport.

ACKNOWLEDGEMENT

This work was partially supported by the French ANR through the projects NANOSIM-GRAPHENE and MIGRAQUEL.

REFERENCES

- [1] C. R. Dean *et al.*, *Boron nitride substrates for high-quality graphene electronics*, Nat. Nanotechnol. **5**, 722 (2010).
- [2] P. J. Zomer, *et al.*, *A transfer technique for high mobility graphene devices on commercially available hexagonal boron nitride*, Appl. Phys. Lett. **99**, 232104 (2011).
- [3] G. Giovannetti *et al.*, *Substrate-induced band gap in graphene on hexagonal boron nitride: ab initio density functional calculations*, Phys. Rev. B. **76**, 073103 (2007).
- [4] N. Kharche and S. K. Nayak, *Quasiparticle band gap engineering of graphene and graphone on Hexagonal Boron nitride substrate*, Nano Lett. **11**, 5274-5278 (2011).
- [5] S. Reich, J. Maultzsch, and C. Thomsen, *Tight-binding description of graphene*, Phys. Rev. B **66**, 035412, 2002.
- [6] A. H. Castro Neto *et al.*, "The electronic properties of graphene", Rev. Mod. Phys. **81**, 109-162 (2009).
- [7] M. I. Katsnelson, K. S. Novoselov, and A. K. Geim, *Chiral tunneling and the Klein paradox in graphene*, Nat. Phys. **2**, 620-625 (2006).
- [8] D. Dragoman and M. Dragoman, *Negative differential resistance of electrons in graphene barrier*, Appl. Phys. Lett. **90**, 143111 (2007).
- [9] V. Nam Do *et al.*, *Electronic transport and spin-polarized effects of relativistic-like particles in graphene structures*, J. Appl. Phys. **104**, 063708 (2008).
- [10] S. J. Han, Z. Chen, A. A. Bol, and Y. Sun, *Channel-length-dependent transport behaviors of Graphene field-effect transistors*, IEEE Electron Device Lett. **32**, 812-814 (2011).

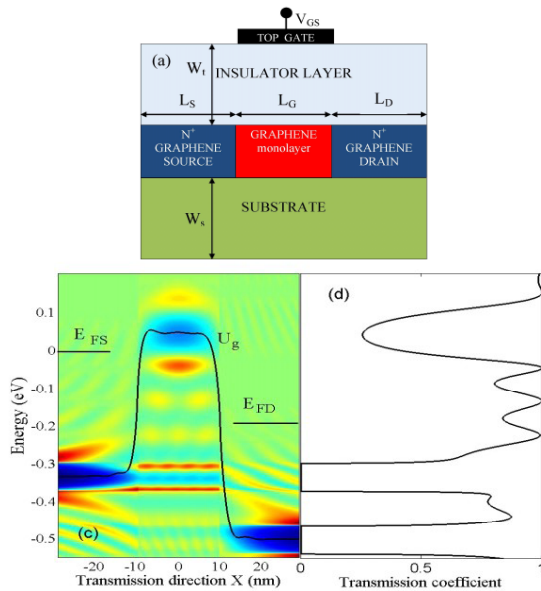


Fig. 1. (a) Schematic view of the simulated GFET. *H*-BN is used as substrate and gate insulator with a dielectric constant $\epsilon_r = 3.5$. (b) Potential profile (solid line) and LDOS for the transverse momentum $k_y = K_y + 6.4 \times 10^7 \text{ m}^{-1}$. E_{FS} and E_{FD} are the Fermi levels in source and drain contacts, respectively. (c) Corresponding transmission coefficient as a function of the energy. Simulation parameters for (b) and (c): $N_D = 10^{13} \text{ cm}^{-2}$, $L_{S,D} = L_G = 20 \text{ nm}$, $W_t = 2 \text{ nm}$, $W_s = 100 \text{ nm}$, $V_{DS} = 0.2 \text{ V}$, $V_{GS} = -0.5 \text{ V}$, $E_{GAP} = 0 \text{ meV}$, and $T = 77 \text{ K}$.

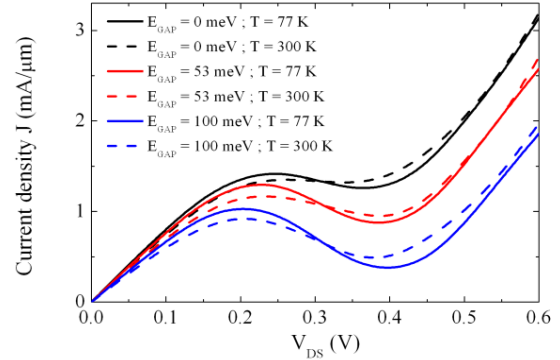


Fig. 2. J - V_{DS} for different bandgap values for $T = 77 \text{ K}$ and $T = 300 \text{ K}$. Simulation parameters: $N_D = 10^{13} \text{ cm}^{-2}$, $L_G = 50 \text{ nm}$, $L_{S,D} = 20 \text{ nm}$, $W_t = 2 \text{ nm}$, $W_s = 100 \text{ nm}$, $V_{GS} = -0.5 \text{ V}$.

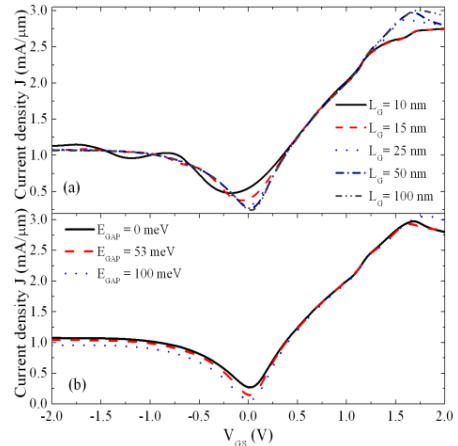


Fig. 3. (a) J - V_{GS} characteristics for different gate lengths. Simulation parameters: $W_t = 2 \text{ nm}$, $W_s = 100 \text{ nm}$, $V_{DS} = 0.1 \text{ V}$, $E_{GAP} = 0 \text{ meV}$ and $T = 77 \text{ K}$. (b) J - V_{GS} characteristics for different energy gaps, with $L_G = 50 \text{ nm}$.

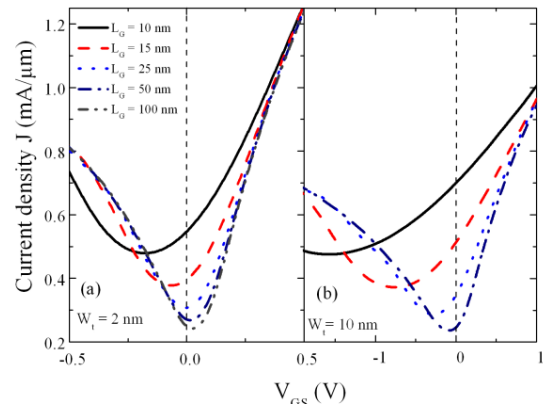


Fig. 4. (a) Zoom of the Fig. 3(a) around the Dirac points in J - V_{GS} characteristics for different L_G with $W_t = 2 \text{ nm}$. (b) Same characteristics but for $W_t = 10 \text{ nm}$. In (a) and (b): $V_{DS} = 0.1 \text{ V}$, $E_{GAP} = 0$, $T = 77 \text{ K}$, $W_s = 100 \text{ nm}$. The vertical dotted lines are guides to the eye.